Nodule-specific Cu^+-chaperone NCC1 is required for symbiotic nitrogen fixation in *Medicago truncatula* root nodules

Cristina Navarro-Gómez[1], Javier León-Mediavilla[1], Hendrik Küpper[2,3], Mario Rodríguez-Simón[1], Alba Paganelli-López[1,4], Jiangqi Wen[5], Stefan Burén[1,4], Kirankumar S. Mysore[5], Syed Nadeem Hussain Bokhari[2], Juan Imperial[1], Viviana Escudero[1,*], Manuel González-Guerrero[1,4,*]

[1]Centro de Biotecnología y Genómica de Plantas. Universidad Politécnica de Madrid (UPM)- Instituto Nacional de Investigación y Tecnología Agraria y Alimentaria (INIA/CSIC). Campus de Montegancedo UPM. 28223 Pozuelo de Alarcón. Spain.

[2]Lab. Plant Biophysics and Biochemistry. Institute of Plant Molecular Biology. Biology Centre. Czech Academy of Sciences. Biology Centre. České Budějovice. Czech Republic.

[3]Dept. Experimental Plant Biology. Faculty of Sciences. University of South Bohemia. České Budějovice. Czech Republic.

[4]Dept. of Biotechnology-Plant Biology. Escuela Técnica Superior de Ingeniería Agraria, Alimentaria y de Biosistemas. Universidad Politécnica de Madrid. 28040 Madrid. Spain.

[5]Institute for Agricultural Biosciences. Oklahoma State University. Ardmore OK73401. USA.

* Corresponding authors: Manuel González-Guerrero (manuel.gonzalez@upm.es)
Viviana Escudero (viviana.escudero@upm.es)

Running title: NCC1 is required for symbiotic nitrogen fixation

ABSTRACT

Cu^+-chaperones are a diverse group of proteins that allocate Cu^+ to specific copper-proteins, creating different copper pools targeted to specific physiological processes. Symbiotic nitrogen fixation carried out in legume root nodules requires relatively large amounts of copper, for which targeted copper deliver systems would be required. MtNCC1 is a nodule-specific Cu^+-chaperone encoded in the *Medicago truncatula* genome, with a N-terminus Atx1-like domain that can bind Cu^+ with picomolar affinities. This gene is expressed primarily from the late infection zone to the early fixation zone, and is located in the cytosol, associated to plasma and symbiosome membranes, and within nuclei. Consistent with its key role in nitrogen fixation, *ncc1* mutants have a severe reduction of nitrogenase activity, and a 50% reduction in copper-dependent cytochrome *c* oxidase activity. A subset of the copper-proteome is also affected in the mutant nodules. Many of these proteins can be pulled-down when using a Cu^+-loaded N-terminal MtNCC1 moiety as a bait, indicating a role in nodule copper homeostasis and in copper-dependent physiological processes. Overall, these data suggest a pleiotropic role of MtNCC1 in copper delivery for symbiotic nitrogen fixation.

Keywords: copper, nitrogen fixation, metallochaperone, nodulation

69 **INTRODUCTION**

70 Copper is an essential nutrient for plants (Marschner and Marschner, 2011). It is
71 involved in key physiological processes such as photosynthesis, respiration, ethylene
72 signalling, or free radical control, among many others (Andresen et al, 2018). This
73 versatile use of copper is largely based on its ability to transition between two redox states
74 (Cu^{+} and Cu^{2+}) in physiological conditions (Burkhead et al., 2009). However, that same
75 property makes copper a toxic reagent at slightly higher concentration, as it can non-
76 enzymatically catalyse Fenton-style reactions producing damaging free radicals
77 (Goldstein et al., 1993). Furthermore, excess copper can displace other essential transition
78 metals from the active site of metalloproteins (Küpper et al., 1996; Küpper et al., 2002;
79 Macomber and Imlay, 2009). As a result, and to prevent copper damage to the cell
80 structures, the "free", hydrated, concentrations of copper in the cytosol are maintained at
81 extremely low levels, less than one ion per cell (Changella, 2003). This is achieved by the
82 coordinated action of small, copper-binding molecules, as well as proteins known as Cu^{+}-
83 chaperones (Robinson and Winge, 2010; Flis et al., 2016).

84 The role of Cu^{+}-chaperones is to deliver copper to different copper-proteins,
85 protecting the cell from copper toxicity (Lin et al., 1997; Wong et al., 2000). Cu^{+}-
86 chaperones bind Cu^{+} with picomolar (pM)- femtomolar (fM) affinity (Rae et al., 1999;
87 Palumaa et al., 2004), which prevents unspecific copper release prior to docking with a
88 compatible protein. This means that metalation is not simply the result of relative copper-
89 binding affinities, but also of the specific protein-protein interaction between donor and
90 acceptor proteins. Consequently, different copper pools are created based on the ability
91 of each protein to interact and exchange copper with one or another Cu^{+}-chaperone.
92 *Saccharomyces cerevisiae* has at least three of these pools: the secretory pathway, that
93 receives copper from Atx1 (Lin et al., 1997); the mitochondrial copper, that obtains it
94 from COX17 (Palumaa et al., 2004); and the Cu, Zn superoxide dismutase that gets it
95 from CCS (Rae et al., 1999). Multicellular organisms are expected to have a larger
96 number of such proteins. Plants have at least a CCS orthologue (Chu et al., 2005), two
97 Cu^{+}-chaperones driving copper to mitochondria (Attallah et al., 2011), another in the
98 stroma (Blaby-Haas et al., 2014), and three ATX1 orthologues with the characteristic
99 Cu^{+}-binding CXXC motive: ATX1 (Shin et al., 2012), CCP (Chai et al., 2020) and CCH
100 (Mira et al., 2001), the later with a C-terminal domain of unknown function. This
101 multiplicity of Cu^{+}-chaperones hints not only at the existence of different copper pools,
102 but also at their specialized roles in plant physiology. For instance, ATX1 seems to be

103 involved in buffering through copper deficiency or excess (Shin et al., 2012), CCH has
104 been proposed to be involved in recovering copper during leave senescence (Mira et al.,
105 2001), and CCP plays a role in plant immunity (Chai et al., 2020). Therefore, it should be
106 expected that other, new Cu^+-chaperones are associated with other copper-dependent
107 processes.

108 While leaves are the main copper sink in most plants during vegetative growth,
109 legumes have a second, major copper sink in their root nodules (Johnston et al., 2001;
110 Senovilla et al., 2018). After the exchange of specific signals between legumes and a
111 group of bacteria known as rhizobia, cells in the root cortex, pericycle and endodermis
112 proliferate to produce nodules (Downie, 2014; Xiao et al., 2014). Concomitant to nodule
113 development, rhizobia penetrate and colonize nodule cells. Surrounded by the plant-
114 derived symbiosome membrane, rhizobia differentiate into bacteroids that synthesize
115 nitrogenase to fix nitrogen. This developmental process can be easily followed in
116 indeterminate type nodules, such as those in pea or in *Medicago truncatula*. Indeterminate
117 nodules maintain their apical meristem over time, leading to a spatial-temporal gradient.
118 As a result, four developmental zones can be observed in these nodules: the apical
119 meristem (zone I), the infection-differentiation zone (zone II), an interzone where oxygen
120 levels drop to prevent nitrogenase inhibition, so that nitrogen fixation can occur in the
121 fixation zone of the nodule (zone III), and a senescent zone (zone IV) in older nodules
122 (Vasse et al., 1990). In exchange for this fixed nitrogen, the host plant provides
123 photosynthates and mineral nutrients, including copper (Udvardi and Poole, 2013;
124 Senovilla et al., 2018).

125 Legume nodules accumulate high levels of copper (around 50 μg/g) (Senovilla et
126 al., 2018), evidencing an important role for this nutrient in nodule development and/or
127 symbiotic nitrogen fixation. Further evidence for this is provided by the existence of a
128 nodule-specific copper uptake transporter, MtCOPT1, that is required for optimal
129 nitrogen fixation and cytochrome oxidase activity of bacteroids (Senovilla et al., 2018).
130 Therefore, it should be expected that specific mechanisms are in place to ensure copper
131 allocation to enzymes involved in symbiotic nitrogen fixation in legume nodules, and that
132 this is achieved via dedicated Cu^+-chaperones. This manuscript provides data supporting
133 this hypothesis, as it reports that *Medtr3g067750* is a nodule-specific Cu^+-chaperone
134 (NCC) that is essential for symbiotic nitrogen fixation.

135

136 **RESULTS**

137 **MtNCC1 is a Cu^+-chaperone**

138 To identify candidate Cu^+-chaperones in *Arabidopsis thaliana* and *M. truncatula*,
139 we collected those sequences annotated as such, as well as those annotated as metal-
140 binding domain proteins or HIPP, removing those that did not contain a CXXC Cu^+-
141 binding motive. Over 30 different candidates were identified in the genomes of these two
142 plant species (Fig. S1). Within *M. truncatula*, there was a nodule-specific candidate,
143 *Medtr3g067750* (NCC1, for Nodule-specific Cu^+-Chaperone1), as indicated by the
144 available transcriptomic databases (Fig. S2). This expression pattern was validated by
145 qRT-PCR analyses (Fig. 1A). Protein modelling showed the existence of two different
146 protein domains: a N-terminal Atx1-like domain comprised by the first 78 amino acids
147 ($MtNCC1_{1-78}$) that included the CXXC motif, and a C-terminal, intrinsically disordered
148 region, with an E-rich motif (Fig. 1B).

149 Yeast complementation assays of the yeast *atx1* mutant were used to determine
150 whether the candidate protein above could function as a Cu^+-chaperone. This strain
151 cannot grow in non-fermentative carbon sources. However, *atx1* showed wild-type
152 growth when expressing *MtNCC1* or $MtNCC1_{1-78}$ (Fig. 1C). To further determine whether
153 MtNCC1 could work as a Cu^+-chaperone, Strep-tagged $MtNCC1_{1-78}$ was purified from
154 *Escherichia coli* (Fig. S3) and used to determine Cu^+-binding stoichiometry and affinity.
155 As expected from an Atx1-like chaperone, $MtNCC1_{1-78}$ bound one Cu^+ per molecule with
156 an affinity constant of 2.45 pM^{-1} (Fig. 1D). Similar stoichiometry was observed after
157 incubating $MtNCC1_{1-78}$ with a 10-fold molar excess of Cu^+ and removing the unbound
158 metal (Fig. S4).

159

160 **MtNCC1 is located in the cytosol and nucleus of nodule cells**

161 To determine whether MtNCC1 was produced in the nodule, promoter-GUS
162 fusions were transformed in *M. truncatula* plants. As shown in Fig 2A, *MtNCC1* was
163 highly expressed in the infection-differentiation zone (ZII), interzone (IZ) and early
164 fixation zone (ZIII) of the nodules, although lower expression levels could be found in
165 older fixation zone areas. This expression pattern is consistent with the transcriptomic
166 data obtained from laser-captured microdissected cells in the Symbimics database (Fig.
167 2B). Moreover, immunolocalization of hemagglutinin epitope (HA)-tagged MtNCC1
168 showed a similar distribution (Fig 2C). Higher magnification images of nodule cells
169 showed MtNCC1-HA in the cytoplasm and in the nuclei in infected and uninfected cells
170 (Fig. 2D). This distribution pattern was not observed in un-transformed plants (Fig. S5).

171 Additionally, MtNCC1$_{1-78}$-HA had the same distribution pattern (Fig. S6). Electron-
172 microscopy images using a gold-conjugated antibody revealed that MtNCC1-HA was
173 found in the cytosol, as well as associated to the plasma and symbiosome membranes
174 (Fig. 2E).
175
176 **MtNCC1 is required symbiotic nitrogen fixation**
177 To determine the physiological role of MtNCC1, an insertional *ncc1* mutant was
178 obtained from a *M. truncatula Tnt1* mutant collection. This line had an insertion in
179 position +1044 that led to loss of *MtNCC1* expression (Fig. 3A). As expected, the mutant
180 line did not present any apparent phenotype under non-symbiotic conditions (Fig S7), but
181 showed a significantly reduced growth and biomass production in symbiosis (Fig. 3B,C).
182 No significant changes in nodule development were observed compared to wild-type
183 plants (Fig. S8). The nitrogenase activity in *ncc1* plants was severely reduced (Fig. 3D).
184 Analyses of *MtNCC1* wild-type *ncc1* segregants suggested that no additional *Tnt1*
185 insertions elsewhere in the genome could explain these phenotypical effects (Fig. S9).
186 Furthermore, growth and nitrogenase activity were restored by introducing a wild-type
187 copy of *MtNCC1* into the mutant line (Fig 3B-D). Finally, cytochrome oxidase activity
188 was significantly reduced in bacteroids, but to a much lower extent than the nitrogenase
189 activity (Fig. 3E).
190
191 ***MtNCC1* mutation affects a subset of the copper-proteome**
192 Consistent with the role of MtNCC1 in copper metabolism, increasing copper
193 concentrations by 10-fold in the nutrient solution was sufficient to restore wild-type
194 growth and nitrogenase activity in *ncc1* plants (Fig. 4). However, overall copper content
195 in the analysed plant organs (roots, shoots, and nodules) was not significantly altered in
196 *ncc1* plants (Fig 5A). Iron levels were not affected either (Fig. 5B). Importantly,
197 metalloproteomic analyses on nodule soluble protein extracts from wild-type and *ncc1*
198 nodules showed reduced copper content in a subset of the proteome (Fig. 6A). The largest
199 differences were found at around 110 kDa and 60 kDa. As this was a separation only by
200 SEC, the copper proteins only represent a small proportion of the total proteins eluting
201 during the times when a maximal difference between the wild-type and *ncc1* samples was
202 observed. This becomes clear when looking at the profiles of other metals at the same
203 time and comparing the UV/VIS spectra with the metal chromatograms (regions of
204 interest in Figures 6B, 6C, complete time range in Figure S10).

205 Therefore, although copper-binding proteins were affected, the total number of proteins
206 contained in two fractions (chosen in the MW ranges of max. differences in copper,
207 Fig 6A) in wild type and *ncc1* nodules remained largely the same (Tables S1 and S2);
208 only 70 out of 1529 proteins in fraction 1 and 12 out of 1900 proteins in fraction 2 missing
209 in *ncc1* compared to wild type. None of the ten most abundant of these differentially
210 expressed proteins have a known role in copper-homeostasis (Table 1). Looking at the
211 entire HPLC-ICPsfMS chromatograms in more detail (Fig S10) reveals additional
212 changes in the metalloproteome that would result from the cross-talk between copper
213 homeostasis and that of other elements. Analysing these changes would be a topic for
214 another study.

215 To further try to identify proteins that would accept Cu^+ by interacting with
216 MtNCC1, Cu^+-loaded $MtNCC1_{1-78}$ ($MtNCC1_{1-78}\cdot Cu^+$) was used as a bait for pull-down
217 assays. To ensure that the identified proteins were those that specifically interacted with
218 $MtNCC1_{1-78}\cdot Cu^+$ and not with the resin, control pull-down assays in which no bait was
219 bound to the resin were done in parallel. The proteins specifically retained by $MtNCC1_{1-}$
220 $_{78}\cdot Cu^+$ are indicated in Table S3. Approximately, one third of these proteins were also
221 present in the selected fractions from the metalloproteomic analyses (Table S4), and
222 mostly they are putatively involved in D-gluconate catabolism, S-adenosylmethione
223 (SAM) cycle, endoplasmatic reticulum unfolded protein response, and protein import into
224 the nucleus. To further confirm some of these interactions, Bi-molecular Fluorescence
225 Complementation (BiFC) studies were carried out in agroinfiltrated tobacco leaves
226 expressing *MtNCC1*$_{1-78}$ together with selected candidates identified in the pull-down
227 experiments. As shown in Fig. 7, $MtNCC1_{1-78}$ interacted with thioredoxin-dependent
228 peroxiredoxin (*Medtr7g105830)*, SAM synthase (*Medtr2g046710),* putative universal
229 stress protein (*Medtr1g088640)*, and pathogenesis-related protein (*Medtr2g076010)*. No
230 signal was observed when $MtNCC1_{1-78}$ was expressed in leaves infiltrated with the empty
231 vectors (Fig. S11).
232

233 **DISCUSSION**

234 Symbiotic nitrogen fixation in legume root nodules is a process that requires of a
235 large transfer of transition elements from the host plant to the root nodules (O'Hara, 2001;
236 González-Guerrero et al., 2016). In recent years, many of the transporters mediating this
237 transfer have been identified (Tejada-Jiménez et al., 2015; Abreu et al., 2017; Tejada-
238 Jiménez et al., 2017; Senovilla et al., 2018; Castro-Rodríguez et al., 2020; Escudero et

239 al., 2020), as well as metal-chelating molecules that maintain metal solubility in saps and
240 apoplast (Kryvoruchko et al., 2018; Escudero et al., 2020b). In the case of copper, there
241 is a high degree of specificity in nodules. Host plants, such as *M. truncatula*, express a
242 nodule-specific Cu^+-uptake transporter, MtCOPT1, to ensure copper uptake by infected
243 cells (Senovilla et al., 2018). Bacteroids also synthesize nodule-specific copper
244 transporters, such as FixI, a P_{1B}-ATPase responsible for providing copper for a nodule-
245 specific high-affinity cytochrome oxidase (Kahn et al., 1989; Preisig et al., 1996).
246 However, an additional level of control based on Cu^+-chaperones must exist so that
247 copper is specifically delivered from very few copper transporters to multiple different
248 copper-enzymes. We have identified MtNCC1 as a representative of this layer of control.
249 The relationship of MtCOPT1 and MtNCC1 roles in nodule copper homeostasis is
250 suggested by the presence of both proteins in the same nodule zones (mainly from late
251 infection to early fixation zones). This hints at a functional pairing between the two
252 proteins, *i.e.* the transporter transfers copper to the chaperone. Moreover, MtNCC1 is not
253 the only copper deliver system to bacteroids. As for *copt1-1*, copper fortification of the
254 nutrient solution is sufficient to restore wild-type growth and nitrogenase activity,
255 suggesting that MtNCC1 is only necessary below a certain copper concentration threshold
256 and that other lower-affinity system(s) can functionally complement MtNCC1.
257 The connection between the reduction of nitrogenase activity and mutation of
258 *MtNCC1* is not direct. Nitrogenase does not use copper as a cofactor, nor is copper known
259 to be directly needed for its synthesis (Burén et al., 2020). In previous studies (Senovilla
260 et al., 2018), reduction of nitrogenase activity could be explained as the consequence of
261 the reduction of cytochrome oxidase activity that would limit the energy available to
262 bacteroids. However, the partial reduction in cytochrome oxidase activity cannot explain
263 the drastic loss of nitrogenase activity in *ncc1*. The explanation cannot be altered nodule
264 morphology either (wild-type and *ncc1* nodules do not seem different), nor can it be a
265 collateral effect on iron metabolism in the nodule. The reason must instead lie in the
266 subset of proteins that interact with MtNCC1. Many of them, when forming complexes
267 with $MtNCC1_{1-78}$ can be detected in the nuclei. Some of them could be involved in
268 epigenetic regulation (SAM synthases) (Liu et al., 2020), in the response to plant-microbe
269 interactions (pathogenesis-related proteins) (Kaur et al., 2017), or in the coordination
270 between host and bacteroid (Nodule-specific Cysteine-rich peptides, NCRs) (Maróti et
271 al., 2015), but their specific roles in symbiotic nitrogen fixation still remain to be
272 determined. Our metalloproteomic and pull-down assays have unveiled a number of new

273 putative copper-proteins that have to be further validated biochemically and in the context
274 of symbiotic nitrogen fixation. Other candidate copper-proteins might emerge from
275 studying the interaction with the C-terminal domain of MtNCC1. However, all our efforts
276 in that direction were fruitless because of our failure to recover either full MtNCC1 or C-
277 domain MtNCC1 from the inclusion bodies that formed when they were expressed in *E.*
278 *coli.*

279 Interestingly, MtNCC1 is not only located in the cytosol or in the proximity of the
280 membranes, it can also be detected in nuclei, as was the case of CCP in Arabidopsis (Chai
281 et al., 2020). However, no nuclear localization signal could be found in the MtNCC1
282 sequence. Alternatively, the observed nuclear localization could be the result from
283 interaction with other proteins. BiFC studies indicate that this is the case, as only some of
284 the interactions tested led to $MtNCC_{1-78}$ detection in nuclei. The migration of MtNCC1
285 from cytosol to nucleus will be likely facilitated by importins (Merkle, 2011), some of
286 which have been detected in the pull-down assays. The physiological relevance of this
287 localization is not evident. Theoretically, copper could be delivered to any proteins in the
288 cytosol and then the newly-metallated proteins could migrate to the nucleus. It could be
289 argued that copper transfer to nucleus could be conditional to specific environmental cues,
290 or that some sort of ternary complex in the nucleus would be needed. These possibilities
291 will have to be specifically tested in the future. However, one role that nuclear MtNCC1
292 does not seem to play is to deliver Cu^+ to a putative copper-sensor. The existence of a
293 nodule-specific copper sensor can be inferred from the previous work on MtCOPT1. Lack
294 of copper uptake by nitrogen-fixing cells did not result in nodules containing less copper,
295 but the opposite (Senovilla et al., 2018). This was interpreted as a copper-deficiency
296 signal being sent from nodule cells, that led to more copper being delivered. However,
297 since MtCOPT1 was not present, this copper did not reach the cell cytosol and
298 accumulated in the apoplast. This phenotype, however, was not observed in *ncc1* mutants,
299 in which no significant change in copper content was observed.

300 In summary, in this work we have shown the existence of a nodule-specific Cu^+-
301 chaperone that is required for nitrogen fixation. We have identified changes in the nodule
302 copper-proteome as a result of losing MtNCC1 activity, as well a new putative copper-
303 proteins that might play a role in symbiotic nitrogen fixation. Future work will be directed
304 to determining the physiological role of these proteins and to verifying that they can
305 accept copper from MtNCC1.
306

307 **METHODS**

308 **Biological materials and growth conditions**

309 *Medicago truncatula* Gaertn R108 seeds were scarified in pure H_2SO_4 for 7.5 min.
310 Then, they were washed with cold water and sterilized with 50% bleach for 1.5 min and
311 imbibed in sterile water in darkness overnight. On the following day, seeds were placed
312 on water-agar plates for 48 h at 4°C, and then allowed to germinate at 22°C for 24 h.
313 Seedlings were planted in sterile perlite pots and inoculated with *Sinorhizobium meliloti*
314 2011 or *S. meliloti* 2011 transformed with pHC60 (Cheng and Walker, 1998), as
315 indicated. Plants were grown in a greenhouse in 16 h light/8 h dark and 22°C and watered
316 with Jenner's solution or water every 2 d, alternatively (Brito et al., 1994). Nodules were
317 collected at 28 days-post-inoculation (dpi). Non-inoculated plants were cultivated in
318 similar conditions, but they were watered every 2 weeks with Jenner's solution
319 supplemented with 2 mM NH_4NO_3. For hairy-root transformations, *M. truncatula*
320 seedlings were infected with *Agrobacterium rhizogenes* ARqua1 carrying the appropriate
321 binary vector as described (Boisson-Dernier et al., 2001). In agroinfiltration experiments,
322 *Nicotiana benthamiana* (tobacco) leaves were infected with the plasmid constructs in *A.*
323 *tumefaciens* GV3101 (Deblaere et al., 1985). Tobacco plants were grown under the same
324 conditions as *M. truncatula*.

325 For yeast complementation assays, *Saccharomyces cerevisiae* strain Δ*atx1* and its
326 parental strain BY4741 (MATa *his3Δ 1 leu2Δ 0 met15Δ 0 ura3Δ 0*) were purchased from
327 the Yeast Knockout Collection (GE Dharmacon). Yeasts were grown in yeast peptone
328 dextrose (YPD) or in synthetic dextrose (SD) media supplemented with 2% glucose
329 (Sherman et al., 1983). Phenotypic characterization was performed in yeast peptone
330 ethanol glycerol (YPEG) medium (Li & Kaplan, 2001).

331 For protein purification, *Escherichia coli* BL21 (DE3) pLysS (Wood, 1966) (*E.*
332 *coli* str. B F–*ompT gal dcm lon hsdSB* ($r_{B-}m_{B-}$) λ(DE3 [*lacI lacUV5-T7p07 ind1 sam7*
333 *nin5*]) [$malB^+$]$_{K-12}$ (λ^S) pLysS [T7p20 ori_{p15A}](Cm^R) was used to produce the required
334 amount of protein.

335

336 **Quantitative real-time RT-PCR**

337 RNA isolation and cDNA synthesis were carried out as previously described
338 (Tejada-Jiménez et al., 2015). Gene expression was studied by quantitative real-time RT-
339 PCR (9700, Applied Biosystems) with primers indicated in Table S5 and normalized to
340 the *M. truncatula Ubiquitin carboxy-terminal hydrolase* gene (*Medtr4g077320*). Real-

341 time cycler conditions have been previously described (González-Guerrero et al., 2010).
342 Determinations were performed with RNA extracted from three independent biological
343 samples, with the threshold cycle determined in triplicate. The relative levels of
344 transcription were determined with the $2^{-\Delta Ct}$ method.
345
346 **Yeast complementation assays**
347 *MtNCC1* and *MtNCC1*$_{1\text{-}78}$ cDNAs were cloned into the yeast expression vector
348 pDR196, between PstI and XhoI restriction sites, by homologous recombination in yeast
349 (primers indicated in Table S5). For yeast transformation, a lithium acetate-based method
350 was used as described (Schiestl and Gietz, 1989). Transformants were selected in SD
351 medium by uracil autotrophy. Phenotypic analysis of yeast transformants were done on
352 YPEG plates (Li & Kaplan, 2001).
353
354 **Protein Expression and Purification.**
355 *MtNCC1*$_{1\text{-}78}$ was obtained by PCR using *MtNCC1* cDNA as the template (primers
356 indicated in Table S5). The resulting cDNA was cloned between *NdeI* and *BamHI*
357 restriction sites in a modified version of pET16b (courtesy of Dr. Luis Rubio). This
358 plasmid adds two N-terminal streptavidin (N-Twin-Strep (N-TS)) tag sequences. Protein
359 expression was induced for 3 h at 37°C by the addition of 1mM IPTG to *E. coli* BL21
360 cells (Wood, 1966). Cells expressing soluble MtNCC1$_{1\text{-}78}$ were disrupted in 100 mM Tris
361 (pH 8.0), 150 mM NaCl (buffer W) using a French press. Homogenates were centrifuged
362 at 54,000 g for 1 h. The protein was purified with a Strep-Tactin XT 4Flow high-capacity
363 column (IBA lifesciences) and stored in 10% glycerol in buffer W at -80°C. Protein
364 quantification was performed in accordance with Bradford assay (Bradford, 1976).
365
366 **Cu^+-binding affinity.**
367 MtNCC1$_{1\text{-}78}$·Cu^+ K_a value was obtained by using a competition assay with BCA
368 followed by colorimetric determination of the BCA_2·Cu^+ complex at 360 nm. MtNCC1$_{1\text{-}}$
369 $_{78}$·Cu^+ K_a was determined by titrating with Cu^+ in a solution of 20 μM BCA, 100 μM
370 MtNCC1$_{1\text{-}78}$ in 50 mM HEPES (pH 7.5), 200 mM NaCl, and 200 μM ascorbate (buffer
371 H). The BCA_2·Cu^+ molar extinction coefficient, ε_{360} = 20,600 cm^{-1} M^{-1}, was determined
372 by titrating μM Cu^+ with 0–10 μM BCA in buffer H. Free metal concentrations were
373 calculated from K_{BCA} = [BCA_2·Cu^+]/[BCA_{free}]^2[Cu^+_{free}], where K_{BCA} is the association

374 constant for $BCA_2 \cdot Cu^+$ (4.60 x 10^{14} M^{-2}) (Yatsunyk and Rosenzweig, 2007; González-
375 Guerrero and Argüello, 2008). The $MtNCC_{1-78} \cdot Cu^+$ K_a value was calculated by using ν
376 = $[Cu^+_{free}]^n K_a/(1 + K_a [Cu^+_{free}]^n)$, where ν is the molar ratio of metal bound to protein and
377 *n* is the number of metal-binding sites. Reported errors for *Ka* and *n* are asymptotic
378 standard errors provided by the fitting software (Origin; OriginLab).
379
380 **GUS staining**
381 *MtNCC1* promoter (*MtNCC1p*; 2 kb upstream of the *MtNCC1* start codon) was
382 amplified using the primers indicated in Table S5, then cloned into pDONR207
383 (Invitrogen) and transferred to pGWB3 vector containing the *GUS* gene (Nakagawa et
384 al., 2007), using Gateway Cloning technology (Invitrogen). *M. truncatula* hairy-roots
385 transformation was carried out as described above. Transformed seedlings were planted
386 in sterile perlite pots and inoculated with *S. meliloti* 2011. GUS activity was measured in
387 nodules of 28 dpi plants as described (Vernoud et al., 2007).
388
389 **Immunolocalization**
390 A DNA fragment containing the full-length *MtNCC1* genomic region and the
391 *MtNCC1p* was cloned into the pGWB13 (Nakagawa et al., 2007)by Gateway technology
392 (Invitrogen). This vector fuses three HA epitopes in the C-terminus of the protein. *M.*
393 *truncatula* hairy-root transformation was carried out as described above (Boisson-Dernier
394 et al., 2001). Transformed seedlings were planted in sterile perlite pots and inoculated
395 with *S. meliloti* 2011 integrating the pHC60 vector that constitutively expresses GFP. 28
396 dpi nodules were collected and fixed in 4% (w/v) paraformaldehyde, 2.5% (w/v) sucrose
397 in phosphate-buffered saline (PBS) at 4°C overnight. Next day, nodules were washed in
398 PBS, and 100-µm sections were generated with a Vibratome 1000 plus (Vibratome).
399 Then, sections were dehydrated using methanol series (30%, 50%, 70% and 100% [v/v]
400 in PBS) for 5 min and then rehydrated. Cell walls were permeabilized with 4% (w/v)
401 cellulase in PBS for 1 h at room temperature and treated with 0.1% (v/v) Tween 20 in
402 PBS for 15 min. Sections were blocked with 5% (w/v) bovine serum albumin (BSA) in
403 PBS and incubated then with an anti-HA mouse monoclonal antibody (Sigma) for 2 h at
404 room temperature. After washing the primary antibody, sections were incubated with an
405 Alexa594-conjugated anti-mouse rabbit monoclonal antibody (Sigma) for 1 h at room
406 temperature. After removing the unbound secondary antibody, DAPI (40,6-diamidino-2-

407 phenylindole) was used to stain the DNA. Images were acquired with a confocal laser-
408 scanning microscope (Leica SP8) using excitation lights at 488 nm for GFP and at 561
409 nm for Alexa 594.
410 For gold-immunolocalization, 28 dpi nodules were collected and fixed in 1%
411 formaldehyde and 0.5% glutaraldehyde in 50 mM potassium phosphate (pH 7.4) for 2 h.
412 The fixation solution was renewed and incubated for an additional 1.5 h. Samples were
413 washed in 50 mM potassium phosphate (pH 7.4) 3 times during 30 min and 3 times for
414 10 min. Nodules were dehydrated by incubating with ethanol dilution series of 30%, 50%,
415 70%, and 90% during 10 min, 96% for 30 min, and 100% for 1 h. Samples were incubated
416 with a series of ethanol and LR-white resin (London Resin Company Ltd, UK) dilutions:
417 1:3 for 3 h, 1:1 overnight, and 3:1 for 3 h, and left in LR-white resin for 48 h. All
418 incubations were done at 4°C. Nodules were placed in gelatine capsules previously filled
419 with LR-white resin and polymerized at 60 °C for 24 h. Ultra-thin sections were cut at
420 Centro Nacional de Microscopia Electrónica (Universidad Complutense de Madrid,
421 Spain) with Reichert Ultracut S-ultramicrotome fitted with a diamond knife. Sections
422 were blocked in 2% bovine serum albumin (BSA) in PBS for 30 min. An anti-HA rabbit
423 monoclonal antibody (Sigma) was used (dilution 1:20 in PBS) as primary antibody.
424 Samples were washed 10 times in PBS for 2 min. As a secondary antibody, 1:150 dilution
425 in PBS of antirabbit goat antibody conjugated to a 15 nm gold particle (BBI solutions)
426 was used. Incubation was performed for 1 h. Sections were washed 10 times with PBS
427 for 2 min and 15 times with water for 2 min. Sections were stained with 2% uranyl acetate
428 and visualized in a JEM 1400 electron microscope at 80 kV.
429
430 **Acetylene reduction assay**
431 Nitrogenase activity was determined by the acetylene reduction assay (Hardy et
432 al., 1968). Nitrogen fixation was analyzed in mutant and control plants at 28 dpi in 30-ml
433 vials fitted with rubber stoppers. Each tube contained one independently transformed
434 plant. Three ml of air inside the vial was replaced by 3 ml of acetylene and then they were
435 incubated at room temperature for 30 min. Gas samples (0.5 ml) were analyzed in a
436 Shimadzu GC-8A gas chromatograph fitted with a Porapak N column. The amount of
437 ethylene produced was determined by measuring the height of the ethylene peak relative
438 to background. After measurements, nodules were collected from roots for weight
439 measurements.
440

441 **Cytochrome oxidase activity**

442 Nodules from 28 dpi plants were collected and used for bacteroid isolation, as
443 described by (Brito et al., 1994) with modifications. Nodules from 50 plants (0.1-0.3 g
444 nodules) were pooled together and crashed with 33% (w/w) of polyvinylpyrrolidone and
445 1 ml of extraction buffer (38 mM K_2HPO_4, 24 mM KH_2PO_4, 2.4 mM $MgCl_2$). Three
446 consecutive centrifugations were performed with the supernatant of the previous one, two
447 at 1000 g (1 and 5 min) and a final one at 5000 g for 10 min. The final pellet was
448 resuspended in 500 µL of resuspension buffer (50 mM HEPES, 200 mM NaCl pH 7).
449 Cytochrome oxidase activity was determined by N,N,N',N'-tetramethyl-p-
450 phenylenediamine (TMPD) oxidation assay. The reaction was started by adding TMPD
451 to the bacteroid sample at a final concentration of 2.7 mM. To obtain the reaction kinetics,
452 each sample was measured at OD_{520} each 10 s for 3 min. To measure protein content to
453 calculate specific activity, the bacteroid suspension was lysed in 10% SDS at 90°C for 5
454 min. The amount of protein was determined with the Pierce™ BCA Protein Assay Kit
455 (Thermo Scientific, Waltham, MA, USA).

456

457 **Metal content determination**

458 To determine metal content, Inductively Coupled Plasma-Mass Spectrometry
459 (ICP-MS) was performed for three independent sets of 28 dpi roots, shoots and nodules
460 pooled from ten plants. ICP-MS was carried out at the Unit of Metal Analysis from the
461 Scientific and Technology Centre, Universidad de Barcelona (Spain). These samples
462 were treated with HNO_3, H_2O_2 and HF in a Teflon reactor at 90°C. The resulting
463 homogenates were diluted with deionized water. Final volumes were calculated by weight
464 and weight: volume ratios. In parallel, samples were digested with three blanks. Metal
465 determination was carried out in an Agilent 7500cw instrument with standard conditions.
466 Calibration was carried out with five solutions prepared from certified NIST standards.

467

468 **Metalloproteomics**

469 Metalloproteomic analyses were performed on 150 28 dpi nodules from wild type
470 or *ncc1* plants. Soluble and membrane proteins were extracted from the nodules as
471 described by Andresen et al. (2016). Afterwards, proteins were separated by size
472 exclusion chromatography coupled to ICP-MS as described (Küpper et al., 2019). Briefly,
473 two Superdex Increase 200 10 x 300 mm and one Superdex Increase 75 10 x 300 mm size
474 exclusion columns were used to separate the nodule protein extracts in 150 mM

475 ammonium bicarbonate buffer with 0.2 mM DDM. Detection was achieved with a
476 customized sector field ICP-MS (Element 2 XR with jet interface and desolvating
477 injection, Thermo Scientific, Bremen Germany) and a diode array detector coupled to a
478 metal-free HPLC system (Azury system. Knauer, Germny). Metal-EDTA complexes in
479 same buffer as the protein extracts were used to calibrate concentration determination. A
480 gel filtration calibration standard (Bio-rad with added PABA) was used to determine size
481 and molecular weight, calibration of metal concentrations in the ICP-MS chromatograms
482 was performed as described in Küpper et al. (2019). Proteins were identified in the
483 Proteomic Unit of Universidad Complutense de Madrid (Spain).
484
485 **Proteomics**
486 Proteomic analyses were performed in the Proteomics Unit of Complutense
487 University of Madrid, a member of Proteored. Samples were liophylized and resuspended
488 in 100 µl of 25 mM ammonium bicarbonate buffer and quantified. Proteins were reduced
489 in 10 mM DTT at 56ºC for 60 min, and subsequently alkylated in 25 mM iodocetamide
490 for 60 min in darkness at room temperature. Samples were digested with Trypsine/LysC
491 protease mix (Pierce, ThermoFisher) at a 1:30 (w/w) ration overnight at 37ºC. Desalted
492 and concentrated peptides were liophylized and reconstituted in 15 µl 2% acetonitrile,
493 0.1% formic acid. One µg of peptides from each sample were analysed by liquid nano-
494 chromatography (Vanquish Neo, Thermo Scientific) coupled to a high-resolution mass
495 spectrometer (Q-Exactive HF (Thermo Scientific). The acquired MS/MS spectra were
496 analysed using Proteome Discoverer 3 (Thermo Scientific) using Mascot 2.8 search
497 engine and the databases SwissProt, *M. truncatula*, *S. meliloti* downloaded from Uniprot.
498 "Correctly" identified proteins are those that have a False Discovery Rate (FDR) below
499 1 % and at least on single peptide identified with high confidence (above 99 %).
500
501 **Pull-down assay**
502 28 grams of fresh *M. truncatula* R108 nodules (from approximately 2.500 plants)
503 were homogenized manually with a mortar and pestle. The homogenate was centrifuged
504 at 20,000 g 4°C for 30 min. To separate soluble from membrane proteins, the supernatant
505 ("cell free" extract) was centrifuged at 100,000 g 4°C for 1 h. The resulting supernatant
506 containing soluble proteins was loaded in Strep-Tactin XT 4Flow High-Capacity column
507 (IBA lifesciences) previously saturated with N-TS-MtNCC$_{1-78}$·Cu^{+}. Co-eluting proteins

were identified by liquid chromatography Mass Spectrometry (LC-MS/MS) at the Proteomic Unit of the Universidad Complutense de Madrid (Spain).

Bimolecular fluorescence complementation

MtNCC1$_{1-78}$ CDS was fused at N-terminus to the N-fragment of YFP (Yellow Fluorescence Protein) in the Gateway vector pNXGW (Kim et al., 2009). The CDS of MtNCC1candidate interactors were fused to the C-fragment of CFP (Cyan Fluorescence Protein) at both N and C-terminus in the Gateway vectors pCXGW and pXCGW (Kim et al., 2009), respectively. Primers for cloning are indicated in Table S5. These constructs were introduced into *A. tumefaciens* GV3101 (Deblaere et al., 1985). *N. benthamiana* leaves were infiltrated as previously described (Senovilla et al., 2018). Leaves were examined after 3 d by confocal laser-scanning microscopy (Zeiss LSM 880) with excitation light of 488 nm for GFP.

Statistical tests

Data were analyzed using Student's unpaired t test to calculate statistical significance of observed differences. Test results with P-values lower than 0.05 were considered as statistically significant.

Data availability

All the data included in this manuscript is available to interested researchers upon request. Proteomics raw data have been deposited in Proteomics Identification Database (PRIDE).

FUNDING

This research was funded by a Ministerio de Ciencia, Innovación y Universidades grant (AGL2018-095996-B-100) to MG-G. CN-G is supported by Formación de Personal de Investigación fellowship PRE2019-089164, and MR-S by Comunidad de Madrid contract from the Plan de Empleo Juvenil (PEJ-2020-TL-BIO-18547). Metalloproteomics studies were funded by the Ministry of Education, Youth and Sports of the Czech Republic with co-financing from the European Union (grant "KOROLID", CZ.02.1.01/0.0/0.0/15_003/0000336), the COST association (grant CA19116 "PLANTMETALS") and the Czech Academy of Sciences (RVO: 60077344) to HK.

Development of the *M. truncatula Tnt1* mutant population was, in part, funded by the National Science Foundation USA grant DBI-0703285.

AUTHOR CONTRIBUTIONS

CN-G performed most of the experimental work in this manuscript. JL-M contributed to the phenotype and confocal immunolocalization work and carried out the GUS, sequence comparison of *A. thaliana* and *M. truncatula* candidate Cu^{+}-chaperones, and the yeast complementation studies. KH and SNHB performed and analysed the metalloproteomic studies. MR-S contributed to plasmid generation and plant management. AP-L collaborated in the BiFC studies. JW and KSM produced and characterized the *M. truncatula Tnt1* collection. SB optimized $MtNCC1_{1-78}$ purification. JI, VE, and MG-G analysed data. VE and MG-G were responsible for overall research supervision and prepared the manuscript with input from all other authors.

ACKNOWLEDGEMENTS

The authors would like to thank Dr. Luis Fernández-Pacios (CBGP, UPM-INIA/CSIC, Spain) for his help with MtNCC1 modelling, and Dr. Luis Oñate (CBGP, UPM-INIA/CSIC, Spain) for giving us the plasmids used for the BiFC assays. We would also like to thank other members of laboratory 279 at Centro de Biotecnología y Genómica de Plantas (UPM-INIA/CSIC) for their support and feedback in preparing this manuscript.

575 **REFERENCES**

576 **Abreu, I., Saez, A., Castro-Rodríguez, R., Escudero, V., Rodríguez-Haas, B.,**
577 **Senovilla, M., Larue, C., Grolimund, D., Tejada-Jiménez, M., Imperial, J., et**
578 **al.** (2017). *Medicago truncatula* Zinc-Iron Permease6 provides zinc to rhizobia-
579 infected nodule cells. *Plant Cell Environ.* **40**:2706–2719.

580 **Andresen, E., Peiter, E., Küpper, H**. (2018). Trace metal metabolism in plants. *J Exp*
581 *Bot* **69:**909-954.

582 **Andresen, E., Kappel, S., Stärk, H.J., Riegger, U., Borovec, J., Mattusch, J., Heinz,**
583 **A., Schmelzer, C.E.H., Matoušková, Š., Dickinson, B., Küpper, H**. (2016).
584 Cadmium toxicity investigated at the physiological and biophysical levels under
585 environmentally relevant conditions using the aquatic model plant *Ceratophyllum*
586 *demersum* L. *New Phytol* **210**:1244-1258

587 **Attallah, C. v., Welchen, E., Martin, A. P., Spinelli, S. v., Bonnard, G., Palatnik, J.**
588 **F., and Gonzalez, D. H.** (2011). Plants contain two SCO proteins that are
589 differentially involved in cytochrome c oxidase function and copper and redox
590 homeostasis. *J Exp Bot* **62**:4281–4294.

591 **Blaby-Haas, C. E., Padilla-Benavides, T., Stübe, R., Argüello, J. M., and Merchant,**
592 **S. S.** (2014). Evolution of a plant-specific copper chaperone family for chloroplast
593 copper homeostasis. *Proc Nat Acad Sci USA* **111**:E5480–E5487.

594 **Boisson-Dernier, A., Chabaud, M., Garcia, F., Bécard, G., Rosenberg, C., and**
595 **Barker, D. G.** (2001). *Agrobacterium rhizogenes*-transformed roots of *Medicago*
596 *truncatula* for the study of nitrogen-fixing and endomycorrhizal symbiotic
597 associations. *Mol Plant Microbe Interact* **14**:695–700.

598 **Bradford, M. M.** (1976). A rapid and sensitive method for the quantitation of microgram
599 quantities of protein utilizing the principle of protein-dye binding. *Anal Biochem*
600 **7**:248–254.

601 **Brito, B., Palacios, J. M., Hidalgo, E., Imperial, J., and Ruiz-Argueso, T.** (1994a).
602 Nickel availability to pea (*Pisum sativum* L.) plants limits hydrogenase activity of
603 *Rhizobium leguminosarum* bv. *viciae* bacteroids by affecting the processing of the
604 hydrogenase structural subunits. *J Bacteriol* **176**:5297–5303.

605 **Burén, S., Jiménez-Vicente, E., Echavarri-Erasun, C., and Rubio, L. M.** (2020).
606 Biosynthesis of nitrogenase cofactors. *Chem Rev* **120**:4921-4968.

607 **Burkhead, J. L., Gogolin Reynolds, K. A., Abdel-Ghany, S. E., Cohu, C. M., and**
608 **Pilon, M.** (2009). Copper homeostasis. *New Phytol.* **182**:799–816.

609 **Castro-Rodríguez, R., Abreu, I., Reguera, M., Novoa-Aponte, L., Mijovilovich, A.,**
610 **Escudero, V., Jiménez-Pastor, F. J., Abadía, J., Wen, J., Mysore, K. S., et al.**
611 (2020). *The Medicago truncatula* Yellow Stripe1-Like3 gene is involved in vascular
612 delivery of transition metals to root nodules. *J Exp Bot* **71**:7257–7269.
613 **Chai, L.-X., Dong, K., Liu, S.-Y., Zhang, Z., Zhang, X.-P., Tong, X., Zhu, F.-F., Zou,**
614 **J.-Z., and Wang, X.-B.** (2020). A putative nuclear copper chaperone promotes plant
615 immunity in Arabidopsis. *J Exp Bot* **71**:6684–6696.
616 **Changella, A.** (2003). Molecular basis of metal-ion selectivity and zeptomolar sensitivity
617 by CueR. *Science* **301**:1383–1397.
618 **Cheng, H. P., and Walker, G. C.** (1998). Succinoglycan is required for initiation and
619 elongation of infection threads during nodulation of alfalfa by *Rhizobium meliloti*. *J*
620 *Bacteriol* **180**:5183–5191.
621 **Chu, C.-C., Lee, W.-C., Guo, W.-Y., Pan, S.-M., Chen, L.-J., Li, H., and Jinn, T.-L.**
622 (2005). A copper chaperone for superoxide dismutase that confers three types of
623 copper/zinc Superoxide dismutase activity in Arabidopsis. *Plant Physiol* **139**:425–
624 436.
625 **Deblaere, R., Bytebier, B., de Greve, H., Deboeck, F., Schell, J., van Montagu, M.,**
626 **and Leemans, J.** (1985). Efficient octopine Ti plasmid-derived vectors for
627 *Agrobacterium*-mediated gene transfer to plants. *Nucleic Acids Res* **13**:4777.
628 **Downie, J. A.** (2014). Legume nodulation. *Curr. Biol.* **24**:R184–R190.
629 **Escudero, V., Abreu, I., Tejada-Jiménez, M., Rosa-Núñez, E., Quintana, J., Prieto,**
630 **R. I., Larue, C., Wen, J., Villanova, J., Mysore, K. S., et al.** (2020a). *Medicago*
631 *truncatula* Ferroportin2 mediates iron import into nodule symbiosomes. *New*
632 *Phytologist* **228**:194–209.
633 **Escudero, V., Abreu, I., del Sastre, E., Tejada-Jiménez, M., Larue, C., Novoa-**
634 **Aponte, L., Castillo-González, J., Wen, J., Mysore, K. S., Abadía, J., et al.**
635 (2020b). Nicotianamine Synthase 2 Is required for symbiotic nitrogen fixation in
636 *Medicago truncatula* nodules. *Front. Plant Sci* **10**.
637 **Flis, P., Ouerdane, L., Grillet, L., Curie, C., Mari, S., and Lobinski, R.** (2016).
638 Inventory of metal complexes circulating in plant fluids: a reliable method based on
639 HPLC coupled with dual elemental and high-resolution molecular mass
640 spectrometric detection. *New Phytol.* **211**:1129–1141.
641 **Goldstein, S., Meyerstein, D., and Czapski, G.** (1993). The Fenton reagents. *Free Radic*
642 *Biol Med* **15**:435–445.

643 **González-Guerrero, M., and Argüello, J. M.** (2008). Mechanism of Cu^+-transporting
644 ATPases: Soluble Cu^+ chaperones directly transfer Cu^+ to transmembrane transport
645 sites. *Proc Natl Acad Sci U S A* **105**:5992-5997.
646 **González-Guerrero, M., Raimunda, D., Cheng, X., and Argüello, J. M.** (2010).
647 Distinct functional roles of homologous Cu^+ efflux ATPases in Pseudomonas
648 aeruginosa. *Mol Microbiol* **78**:1246-1258.
649 **González-Guerrero, M., Escudero, V., Sáez, Á., and Tejada-Jiménez, M.** (2016).
650 Transition metal transport in plants and associated endosymbionts. Arbuscular
651 mycorrhizal fungi and rhizobia. *Front. Plant Sci.* **7**:1088.
652 **Hardy, R. W. F., Holsten, R. D., Jackson, E. K., and Burns, R. C.** (1968). The
653 acetylene-ethylene assay for N_2 Fixation: Laboratory and field evaluation. *Plant*
654 *Physiol* **43**:1185–1207.
655 **Johnston, A. W., Yeoman, K. H., and Wexler, M.** (2001). Metals and the rhizobial-
656 legume symbiosis - uptake, utilization and signalling. *Adv. Microb. Physiol* **45**:113–
657 156.
658 **Kahn, D., David, M., Domergue, O., Daveran, M. L., Ghai, J., Hirsch, P. R., and**
659 **Batut, J.** (1989). *Rhizobium meliloti fixGHI* sequence predicts involvement of a
660 specific cation pump in symbiotic nitrogen fixation. *J Bacteriol* **171**:929–939.
661 **Kaur, A., Pati, P. K., Pati, A. M., and Nagpal, A. K.** (2017). In-silico analysis of cis-
662 acting regulatory elements of pathogenesis-related proteins of *Arabidopsis thaliana*
663 and *Oryza sativa*. *PLoS One* **12**:e0184523.
664 **Kim, J. G., Li, X., Roden, J. A., Taylor, K. W., Aakre, C. D., Su, B., Lalonde, S.,**
665 **Kirik, A., Chen, Y., Baranage, G., et al.** (2009). *Xanthomonas* T3S effector XopN
666 suppresses PAMP-triggered immunity and interacts with a tomato atypical
667 Receptor-Like Kinase and TFT1. *Plant Cell* **21**:1305-1323.
668 **Kryvoruchko, I. S., Routray, P., Sinharoy, S., Torres-Jerez, I., Tejada-Jiménez, M.,**
669 **Finney, L. A., Nakashima, J., Pislariu, C. I., Benedito, V. A., González-**
670 **Guerrero, M., et al.** (2018). An iron-activated citrate transporter, MtMATE67, is
671 required for symbiotic nitrogen fixation. *Plant Physiol* **176**:2315–2329.
672 **Küpper, H., Küpper, F., Spiller, M.** (1996). Environmental relevance of heavy metal
673 substituted chlorophylls using the example of submersed water plants. *J Exp Bot*
674 **47:**259-266.

675 **Küpper, H., Šetlík, I., Spiller, M., Küpper F.C., Prášil, O.** (2002). Heavy metal-
676 induced inhibition of photosynthesis: targets of in vivo heavy metal chlorophyll
677 formation. *J Phycol* **38:**429-441.
678 **Küpper, H., Andresen, E**. (2016). Mechanisms of metal toxicity in plants. *Metallomics*
679 **8**:269-285.
680 **Küpper, H., Bokhari, S. N. H., Jaime-Pérez, N., Lyubenova, L., Ashraf, N., and**
681 **Andresen, E.** (2019). Ultratrace metal speciation analysis by coupling of sector-
682 field ICP-MS to high-resolution size exclusion and reversed-phase liquid
683 chromatography. *Anal Chem* **91**:10961–10969.
684 **Li, L., and Kaplan, J.** (2001). The yeast gene MSC2, a member of the Cation Diffusion
685 Facilitator family, affects the cellular distribution of zinc. *J Biol Chem* **276**:5036–
686 5043.
687 **Lin, S.-J., Pufahl, R. A., Dancis, A., O'Halloran, T. v, and Culotta, V. C.** (1997). A
688 role for the *Saccharomyces cerevisiae* ATX1 gene in copper trafficking and iron
689 transport. *J Biol Chem* **272**:9215–9220.
690 **Liu, M., Saha, N., Gajan, A., Saadat, N., Gupta, S. v., and Pile, L. A.** (2020). A
691 complex interplay between SAM synthetase and the epigenetic regulator SIN3
692 controls metabolism and transcription. *J Biol Chem* **295**:375–389.
693 **Macomber, L., and Imlay, J. A.** (2009). The iron-sulfur clusters of dehydratases are
694 primary intracellular targets of copper toxicity. *Proc. Natl. Acad. Sci. U S A*
695 **106**:8344–8349.
696 **Maróti, G., Downie, J. A., and Kondorosi, E.** (2015). Plant cysteine-rich peptides that
697 inhibit pathogen growth and control rhizobial differentiation in legume nodules.
698 *Curr Opin Plant Biol* **26**:57–63.
699 **Marschner, H., and Marschner, P.** (2011). *Marschner's Mineral Nutrition of Higher*
700 *Plants*. Elsevier Science.
701 **Merkle, T.** (2011). Nucleo-cytoplasmic transport of proteins and RNA in plants. *Plant*
702 *Cell Rep* **30**:153–176.
703 **Mira, H., Martínez-García, F., and Peñarrubia, L.** (2001). Evidence for the plant-
704 specific intercellular transport of the Arabidopsis copper chaperone CCH. *Plant J.*
705 **25**:521–528.
706 **Nakagawa, T., Kurose, T., Hino, T., Tanaka, K., Kawamukai, M., Niwa, Y.,**
707 **Toyooka, K., Matsuoka, K., Jinbo, T., and Kimura, T.** (2007). Development of

708 series of gateway binary vectors, pGWBs, for realizing efficient construction of
709 fusion genes for plant transformation. *J Biosci Bioeng* **104**:34–41.
710 **O'Hara, G. W.** (2001). Nutritional constraints on root nodule bacteria affecting
711 symbiotic nitrogen fixation: a review. *Aust. J. Exp. Agr.* **41**:417–433.
712 **Palumaa, P., Kangur, L., Voronova, A., and Sillard, R.** (2004). Metal-binding
713 mechanism of Cox17, a copper chaperone for cytochrome c oxidase. *Biochem J*
714 **382**:307–314.
715 **Preisig, O., Zufferey, R., Thony-Meyer, L., Appleby, C. A., and Hennecke, H.** (1996).
716 A high-affinity cbb3-type cytochrome oxidase terminates the symbiosis- specific
717 respiratory chain of *Bradyrhizobium japonicum*. *J. Bacteriol.* **178**:1532–1538.
718 **Rae, T. D., Schmidt, P. J., Pufahl, R. A., Culotta, V. C., and v. O'Halloran, T.** (1999).
719 Undetectable intracellular free copper: The requirement of a copper chaperone for
720 superoxide dismutase. *Science* **284**:805–808.
721 **Robinson, N. J., and Winge, D. R.** (2010). Copper metallochaperones. *Annu. Rev.*
722 *Biochem.* **79**:537–562.
723 **Schiestl, R. H., and Gietz, R. D.** (1989). High efficiency transformation of intact yeast
724 cells using single stranded nucleic acids as a carrier. *Curr Genet* **16**:339–346.
725 **Senovilla, M., Castro-Rodríguez, R., Abreu, I., Escudero, V., Kryvoruchko, I.,**
726 **Udvardi, M. K., Imperial, J., and González-Guerrero, M.** (2018). *Medicago*
727 *truncatula* copper transporter 1 (MtCOPT1) delivers copper for symbiotic nitrogen
728 fixation. *New Phytologist* **218**:696–709.
729 **Sherman, Fred., Fink, G. R., Hicks, J. B., and Cold Spring Harbor Laboratory.**
730 (1983). Methods in yeast genetics. Cold Spring Harbour Lab.
731 **Shin, L.-J., Lo, J.-C., and Yeh, K.-C.** (2012). Copper chaperone antioxidant protein1 is
732 essential for copper homeostasis. *Plant Physiol* **159**:1099–1110.
733 **Tejada-Jiménez, M., Castro-Rodríguez, R., Kryvoruchko, I., Mercedes Lucas, M.,**
734 **Udvardi, M., Imperial, J., and González-Guerrero, M.** (2015). *Medicago*
735 *truncatula* Natural Resistance-Associated Macrophage Protein1 is required for iron
736 uptake by rhizobia-infected nodule cells. *Plant Physiol* **168**:258–272.
737 **Tejada-Jiménez, M., Gil-Diez, P., Leon-Mediavilla, J., Wen, J., Mysore, K. S.,**
738 **Imperial, J., and Gonzalez-Guerrero, M.** (2017). *Medicago*
739 *truncatula* Molybdate Transporter type 1 (MOT1.3) is a plasma membrane
740 molybdenum transporter required for nitrogenase activity in root nodules under
741 molybdenum deficiency. *New Phytol* **216**:1223–1235.

742 **Udvardi, M., and Poole, P. S.** (2013). Transport and metabolism in legume-rhizobia
743 symbioses. *Annu Rev Plant Biol* **64**:781–805.
744 **Vasse, J., de Billy, F., Camut, S., and Truchet, G.** (1990). Correlation between
745 ultrastructural differentiation of bacteroids and nitrogen fixation in alfalfa nodules.
746 *J. Bacteriol.* **172**:4295–4306.
747 **Vernoud, V., Journet, E. P., and Barker, D. G.** (2007). MtENOD20, a Nod factor-
748 inducible molecular marker for root cortical cell activation. *Mol Plant Microbe*
749 *Interact* **12**:604–614.
750 **Wong, P. C., Waggoner, D., Subramaniam, J. R., Tessarollo, L., Bartnikas, T. B.,**
751 **Culotta, V. C., Price, D. L., Rothstein, J., and Gitlin, J. D.** (2000). Copper
752 chaperone for superoxide dismutase is essential to activate mammalian Cu/Zn
753 superoxide dismutase. *Proc Nat Acad Sci USA* **97**:2886–2891.
754 **Wood, W. B.** (1966). Host specificity of DNA produced by Escherichia coli: bacterial
755 mutations affecting the restriction and modification of DNA. *J Mol Biol* **16**:118–
756 133.
757 **Xiao, T. T., Schilderink, S., Moling, S., Deinum, E. E., Kondorosi, E., Franssen, H.,**
758 **Kulikova, O., Niebel, A., and Bisseling, T.** (2014). Fate map of *Medicago*
759 *truncatula* root nodules. *Development* **141**:3517–3528.
760 **Yatsunyk, L. A., and Rosenzweig, A. C.** (2007). Cu(I) binding and transfer by the N
761 terminus of the Wilson disease protein. *J Biol Chem* **282**:8622–8631.
762
763
764
765
766
767
768
769
770
771
772
773
774
775

776 **FIGURE LEGENDS**

777 **Figure 1. MtNCC1 is a nodule-specific Cu^+-chaperone.** A, *MtNCC1* expression in *S.*
778 *meliloti*-inoculated (roots, shoots, and nodules) and non-inoculated (roots and shoots)
779 plants relative to standard gene *Ubiquitin carboxyl-terminal hydrolase.* Data are the mean
780 ± SE of three independent experiments with five pooled plants. B, Predicted structure of
781 MtNCC1. The classical Atx1-like domain is indicated in pink, with the two conserved
782 Cu^+-binding cysteines (C22 and 25). The glutamate-rich region in the C-terminal domain
783 is indicated with wireframes. C, Parental strain BY4741 was transformed with empty
784 pDR196 vector, while the Δatx1 mutant NCC1 was transformed with empty pDR196 or
785 containing MtNCC1 or $MtNCC1_{1-78}$. D, Cu^+ binding to $MtNCC1_{1-78}$ determined in
786 competition assays with BCA. The data were fit using n = 1.03 ± 0.04 Cu^+ per protein
787 and $K_a = 2{,}45 \cdot 10^{-12} \pm 3.44 \cdot 10^{-13}$ M^{-1}. Data are the mean ± SE (n = 3).

788

789 **Figure 2. Localization of MtNCC1 in *M. truncatula* nodules.** A, GUS staining of 28
790 dpi nodules expressing the *gus* gene under the control of the *MtNCC1* promoter region.
791 Left panel shows the whole nodule and right panel shows a longitudinal section with the
792 different developmental zones indicated. Bars = 400 µm. B, *MtNCC1* expression in the
793 different nodule zones as indicated in the Symbimics database
794 (http://ia.nt.toulouse.inra.fr/symbimics/). ZI: zone I; ZIIp: zone II proximal; ZIId: zone
795 II distal; IZ: interzone; ZII: zone III. C, Longitudinal section of 28 dpi *M. truncula*
796 nodules expressing *MtNCC1* fused to three HA domains driven by its own promoter. HA-
797 tagged proteins were detected with using an Alexa594 conjugated antibody (red, left
798 panel). Nodules were colonized by a GFP-expressing *S. meliloti* (green, central panel).
799 DNA was stained with DAPI (blue) and overlaid with the previous two channels and the
800 transillumination signal (right panel). Bars = 100 µm. D, Closer view of rhizobia-infected
801 cell in zone II. Bars = 10 µm. E, Immunolocalization of MtNCC1-HA in 28 dpi nodules
802 using gold-conjugated antibodies and electron transmission microscopy. Gold particles
803 are indicated by arrows and asterisks represent bacteroids. PM indicates Plasma
804 membrane, and Mit refers to mitochondria. Bars = 1µm.

805

806 **Figure 3. MtNCC1 is required for nitrogen fixation**. A, Amplification of *MtNCC1*
807 transcript by RT-PCR in 28 dpi nodules of wild type and *ncc1* mutants. *MtUb1* (*Ubiquitin*
808 *carboxyl-terminal hydrolase 1*) was used as a constitutive gene. B, Growth of

809 representative plants of wild type (WT), *ncc1* mutant and *ncc1* mutants transformed with
810 *MtNCC1* regulated by its own promoter. Bar = 1cm. C, Fresh weight of shoots and roots
811 of WT, *ncc1* and *ncc1* transformed with *MtNCC1* regulated by its own promoter. Data
812 are the mean ± SE (n = 15). D, Acetylene reduction assay in 28 dpi nodules from WT,
813 *ncc1* mutants and *ncc1* transformed with *MtNCC1* regulated by its own promoter. Data
814 are the mean ± SE (n = 7-13). E, Cytochrome oxidase (COX) activity in bacteroids
815 isolated from 28 dpi nodules of WT and *ncc1* mutant plants. Data are the mean ± SE of
816 at least three sets of 35-40 pooled plants each. Student's *t*-test was used for statistical
817 analysis (* = P≤ 0.05).
818
819 **Figure 4. Copper supplementation complements the *ncc1* phenotype.** A, Growth of
820 representative plants of wild type (WT) and *ncc1* mutant watered with standard copper
821 concentrations (0.16 μM) and copper excess (1.6 μM). Bar = 1cm. B, Fresh weight of
822 shoots and roots of WT and *ncc1* mutant watered with standard copper concentrations
823 (0.16 μM) and copper excess (1.6 μM). Data are the mean ± SE (n = 16-23). C, Acetylene
824 reduction assay in 28 dpi nodules from WT and *ncc1* mutant watered with standard copper
825 concentrations (0.16 μM) and copper excess (1.6 μM). Data are the mean ± SE (n = 16-
826 23). All comparison were done to WT samples using Student's *t*-test (* = P≤ 0.05).
827
828 **Figure 5. Mutation of *MtNCC1* does not alter the nodule metallome.** A, Copper
829 content in 28 dpi shoots, roots and nodules of wild type (WT) and *ncc1* plants. Data are
830 the mean ± SE of three sets of ten pooled plants. B, Iron content in 28 dpi shoots, roots
831 and nodules of wild type (WT) and *ncc1* plants. Data are the mean ± SE of three sets of
832 ten pooled plants. C, Normalized HPLC-ICPsfMS determinations of copper content in
833 two independent biological replicates of 28 dpi WT and *ncc1* nodules. Fractions subjected
834 to proteomic analyses are boxed and indicated as F1 and F2.
835
836 **Figure 6. Mutation of *MtNCC1* alters the nodule copper-proteome.** A,
837 Metalloproteomics by HPLC-ICPsfMS. The normalized chromatograms show copper
838 content in two independent biological replicates of 28 dpi WT and *ncc1* nodules.
839 Fractions subjected to proteomic analyses are boxed and indicated as F1 and F2. B and
840 C, Comparison of the most important element chromatograms and UV/VIS absorption
841 DAD in the chromatogram region where the biggest differences between the mutant had

been seen in the copper chromatogram. B, replicate 1 of the WT, C, replicate 1 of the *ncc1* mutant.

Figure 7. **Bimolecular Fluorescent Complementation assays of MtNCC1$_{1-78}$ interactions.** Transient co-expression of MtNCC1$_{1-78}$ in pNXGW and candidate proteins thioredoxin-dependent peroxiredoxin (A) and SAM synthase (B) in pCXGW, putative universal stress protein (C) and pathogenesis-related protein (D) in pXCGW, in *N. benthamiana* leaf cells 3 days-post-agroinfiltration. Left panel corresponds to the fluorescent signal of MtNCC1$_{1-78}$ and corresponding interactor (green); central panel, transillumination; right panel, overlaid fluorescent image and transillumination images. Bars = 20 μm.

876 **TABLES**

877 **Table 1**. Top ten most abundant proteins detected in wild type replicates and not in *ncc1*
878 replicates in Fractions 1 or 2 of the metalloproteomic analyses of nodule soluble proteins.

Uniprot Accesion	Organism	Description	Fraction
Q4H1G3	*M. truncatula*	S-adenosylmethionine synthase	1
A0A072U7P3	*M. truncatula*	Heat shock cognate 70 kDa protein	1
P47923	*M. truncatula*	Nucleoside diphosphate kinase 2	1
Q1SL05	*M. truncatula*	Putative small GTPase superfamily, P-loop containing nucleoside triphosphate hydrolase	2
G7IEZ9	*M. truncatula*	Chalcone-flavonone isomerase family protein 2	1
Q92M81	*S. meliloti*	Glyceraldehyde-3-phosphate dehydrogenase	1
A0A072UDY2	*M. truncatula*	Presequence protease	1
Q92SW9	*S. meliloti*	Recombination protein Rec	2
Q92RK3	*S. meliloti*	4-phospho-D-erythronate dehydrogenase	1
Q92RH2	*S. meliloti*	3,4-dihydroxy-2-butanone 4-phosphate synthase	1

879

Figure 1

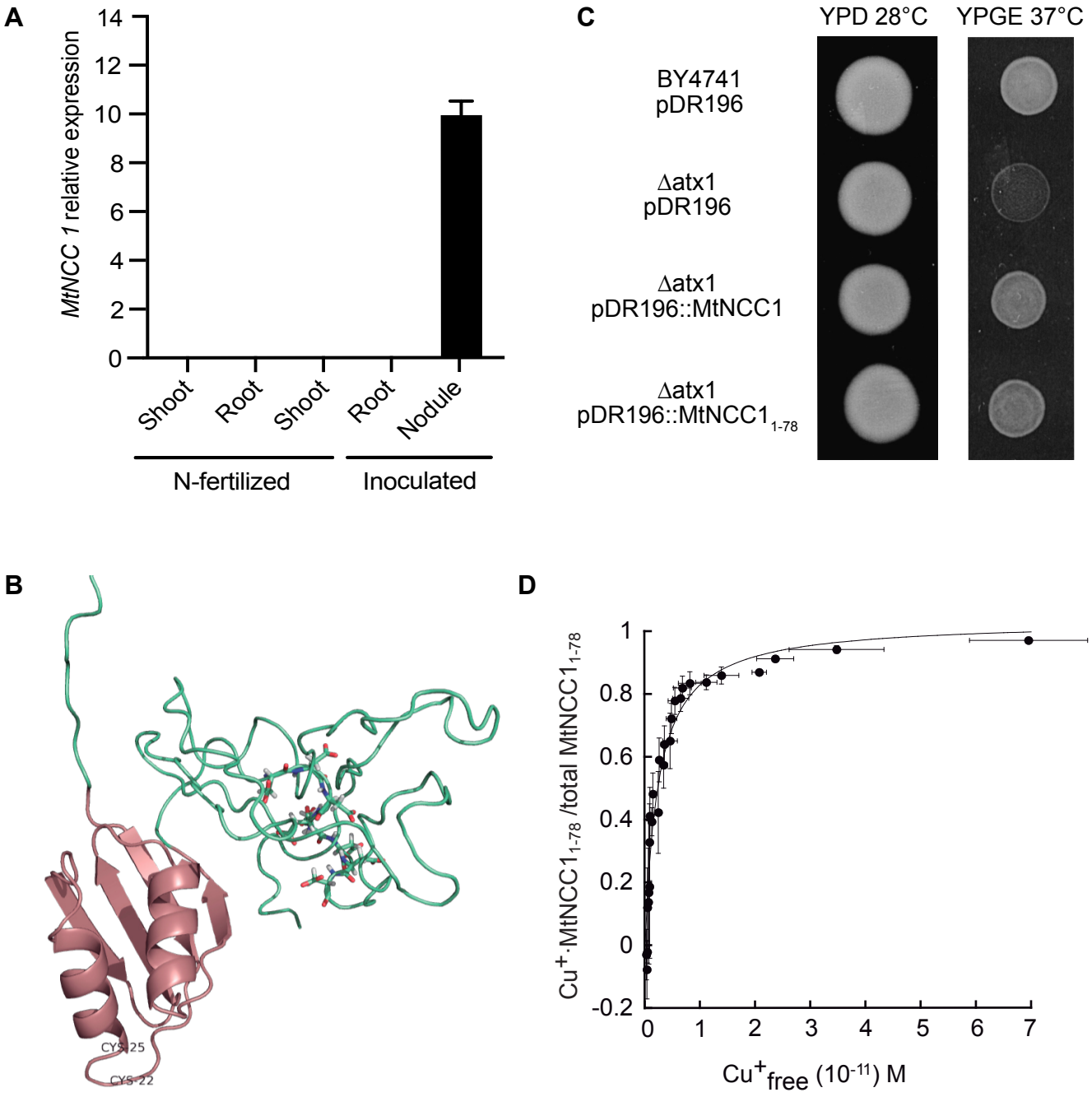
A
MtNCC 1 relative expression
14
12
10
8
6
4
2
0
Shoot
Root
Shoot
Root
Nodule
N-fertilized
Inoculated
C
YPD 28°C
YPGE 37°C
BY4741
pDR196
Δatx1
pDR196
Δatx1
pDR196::MtNCC1
Δatx1
pDR196::MtNCC1 1-78
B
CYS 25
CYS 22
D
Cu+·MtNCC1 1-78 /total MtNCC1 1-78
1
0.8
0.6
0.4
0.2
0
-0.2
0
1
2
3
4
5
6
7
Cu+free (10-11) M

Figure 2

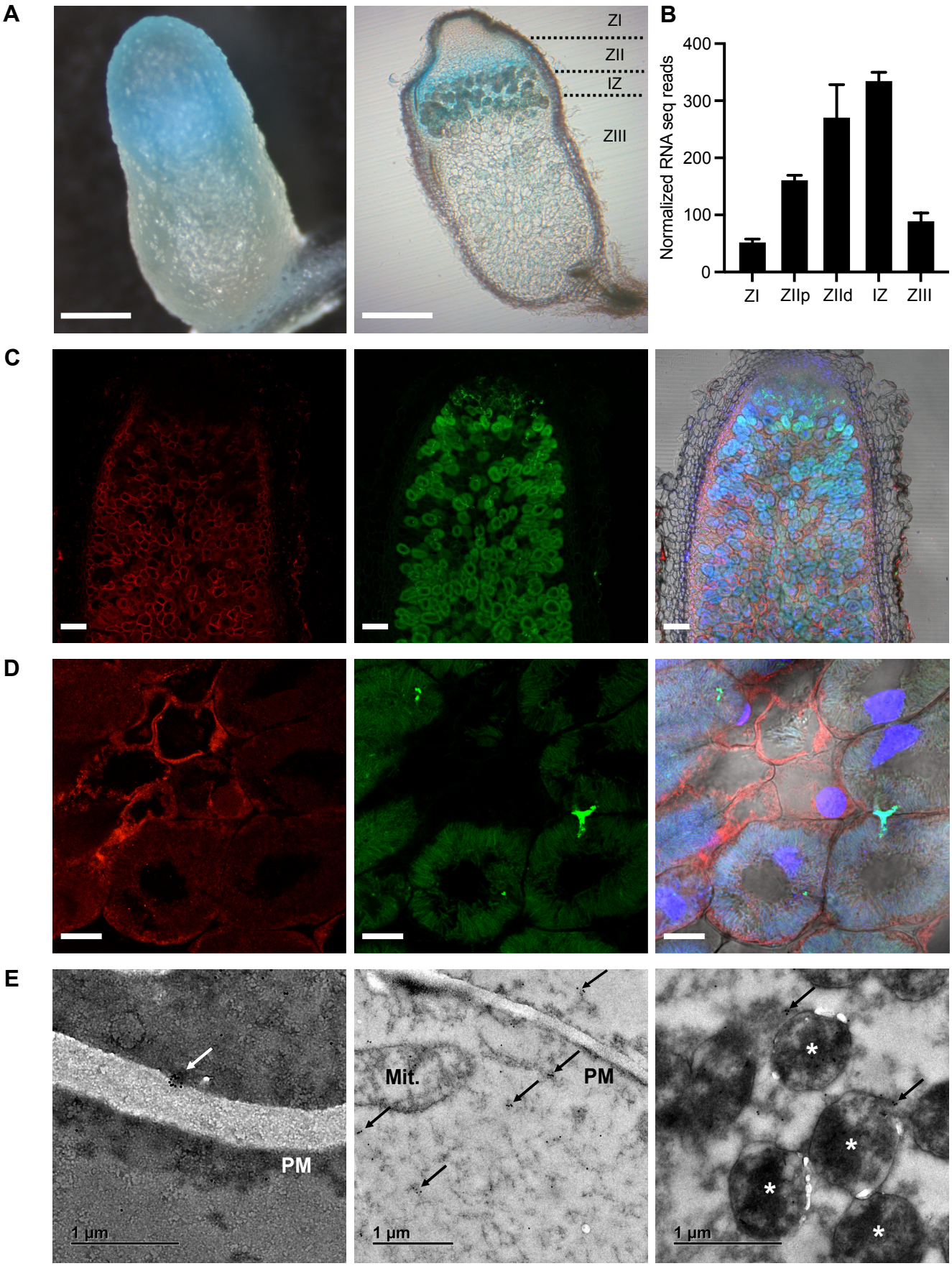
A
ZI
ZII
IZ
ZIII
B
Normalized RNA seq reads
400
300
200
100
0
ZI
ZIIp
ZIId
IZ
ZIII
C
D
E
PM
1 µm
Mit.
PM
1 µm
1 µm

Figure 3

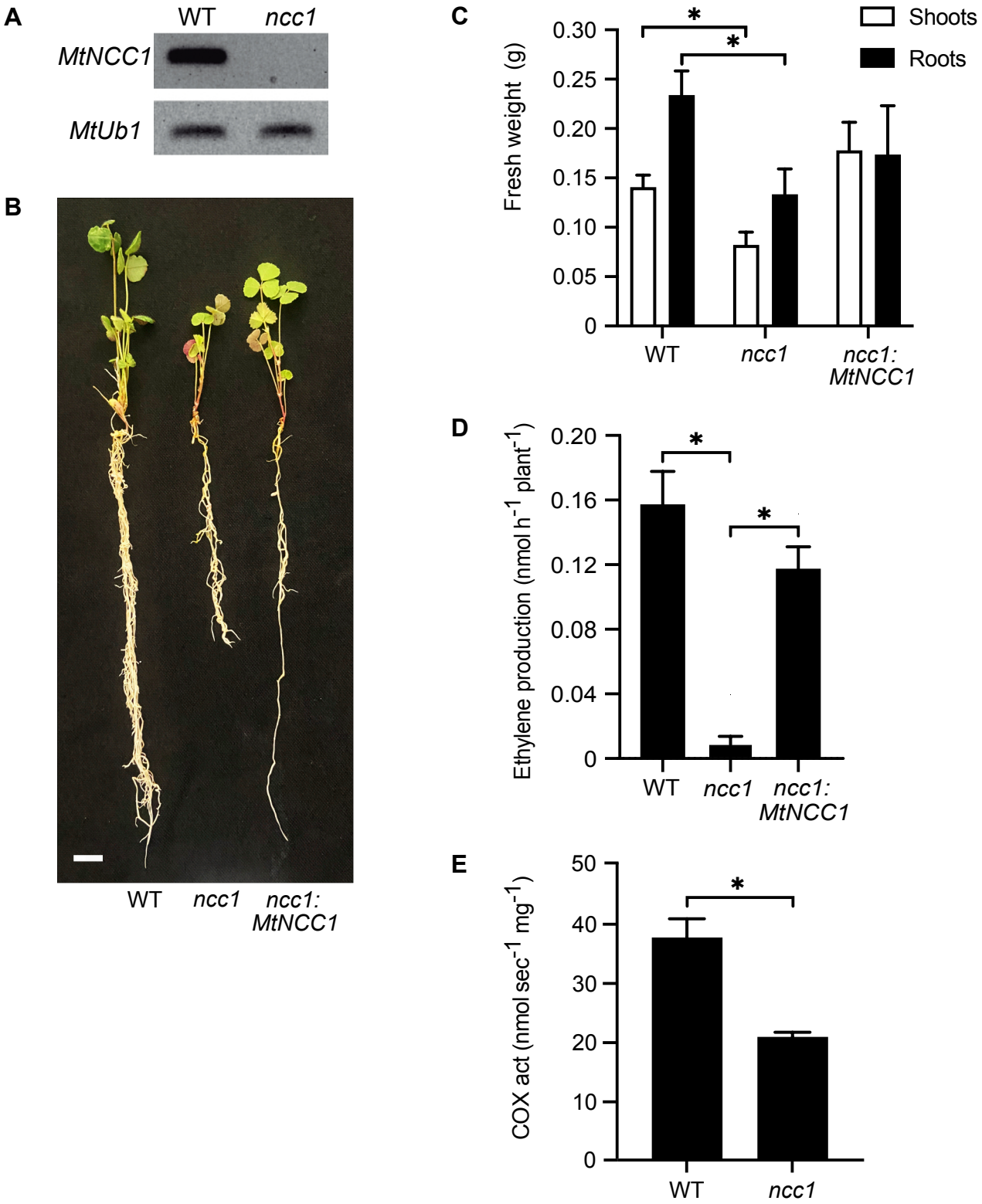
A
WT
ncc1
MtNCC1
MtUb1
B
WT
ncc1
ncc1:
MtNCC1
C
Shoots
Roots
Fresh weight (g)
0.30
0.25
0.20
0.15
0.10
0.05
0
*
*
WT
ncc1
ncc1:
MtNCC1
D
Ethylene production (nmol h-1 plant-1)
0.20
0.16
0.12
0.08
0.04
0
*
*
WT
ncc1
ncc1:
MtNCC1
E
COX act (nmol sec-1 mg-1)
50
40
30
20
10
0
*
WT
ncc1

Figure 4

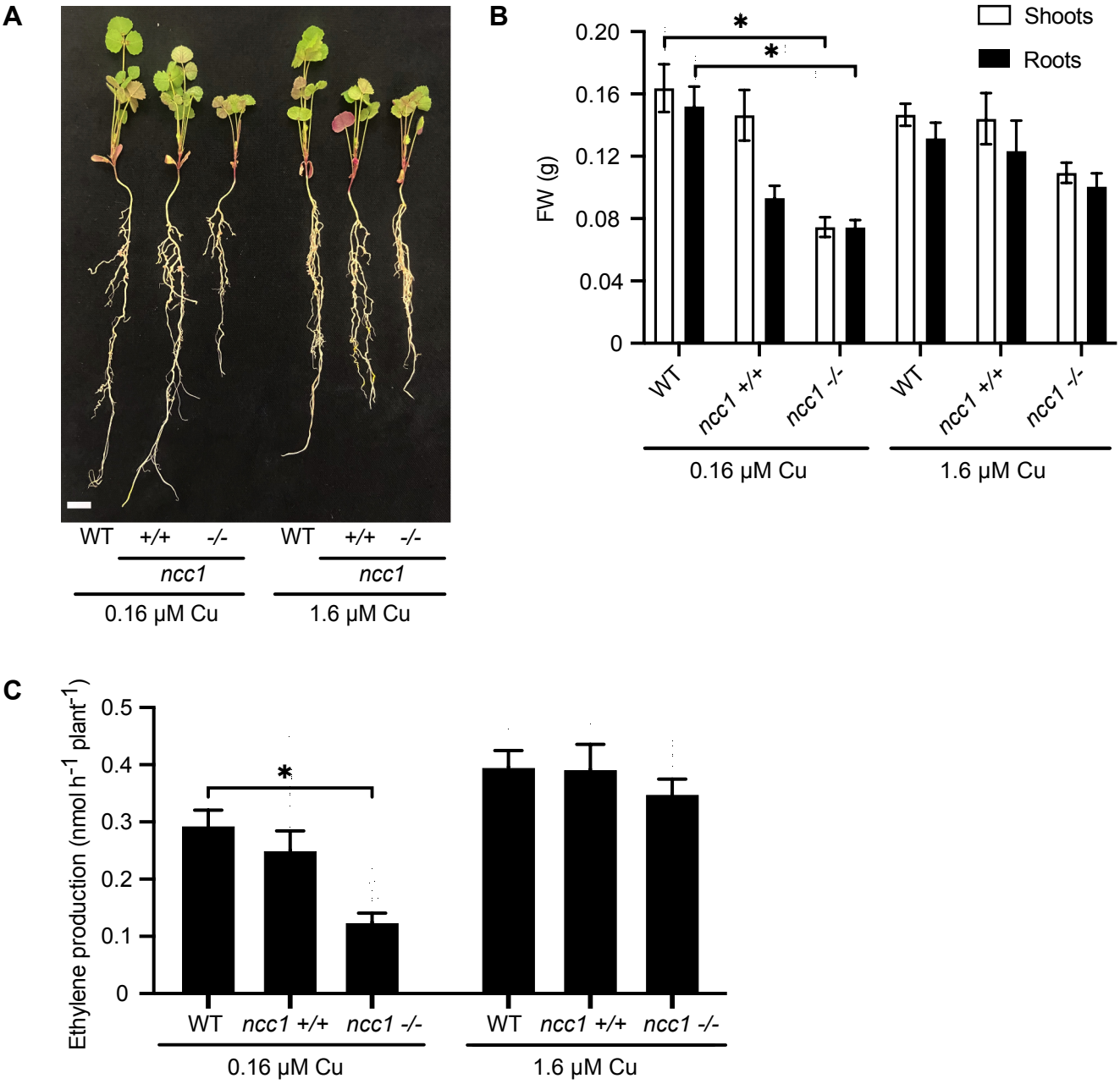
A
WT
+/+
-/-
ncc1
0.16 µM Cu
WT
+/+
-/-
ncc1
1.6 µM Cu
B
Shoots
Roots
FW (g)
0.20
0.16
0.12
0.08
0.04
0
*
*
WT
ncc1 +/+
ncc1 -/-
WT
ncc1 +/+
ncc1 -/-
0.16 µM Cu
1.6 µM Cu
C
Ethylene production (nmol h-1 plant-1)
0.5
0.4
0.3
0.2
0.1
0
*
WT
ncc1 +/+
ncc1 -/-
WT
ncc1 +/+
ncc1 -/-
0.16 µM Cu
1.6 µM Cu

Figure 5

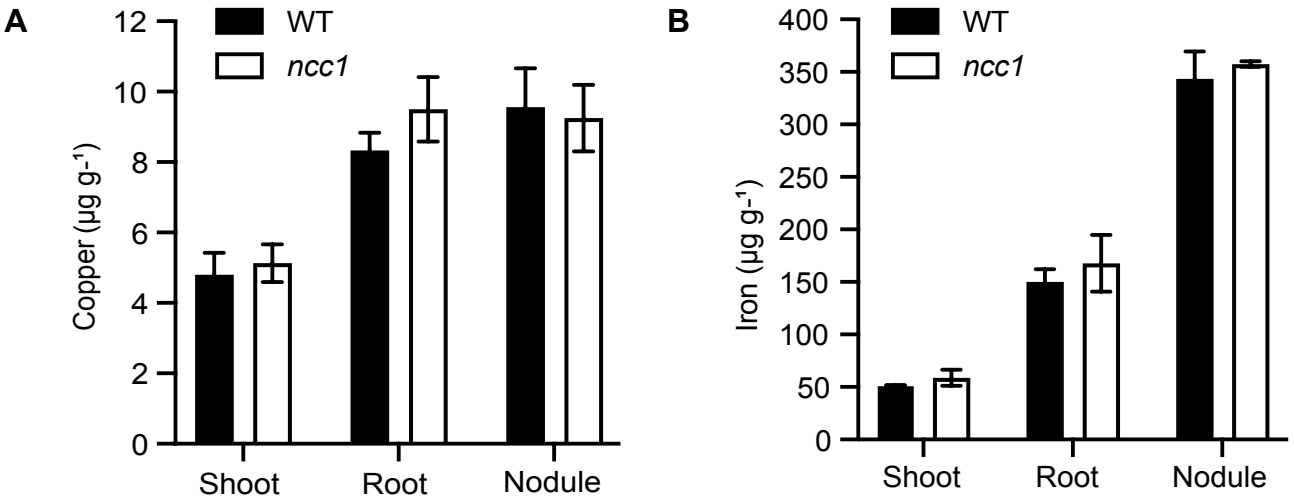
A
WT
ncc1
Copper (µg g-1)
0
2
4
6
8
10
12
Shoot
Root
Nodule
B
WT
ncc1
Iron (µg g-1)
0
50
100
150
200
250
300
350
400
Shoot
Root
Nodule

Figure 6

A

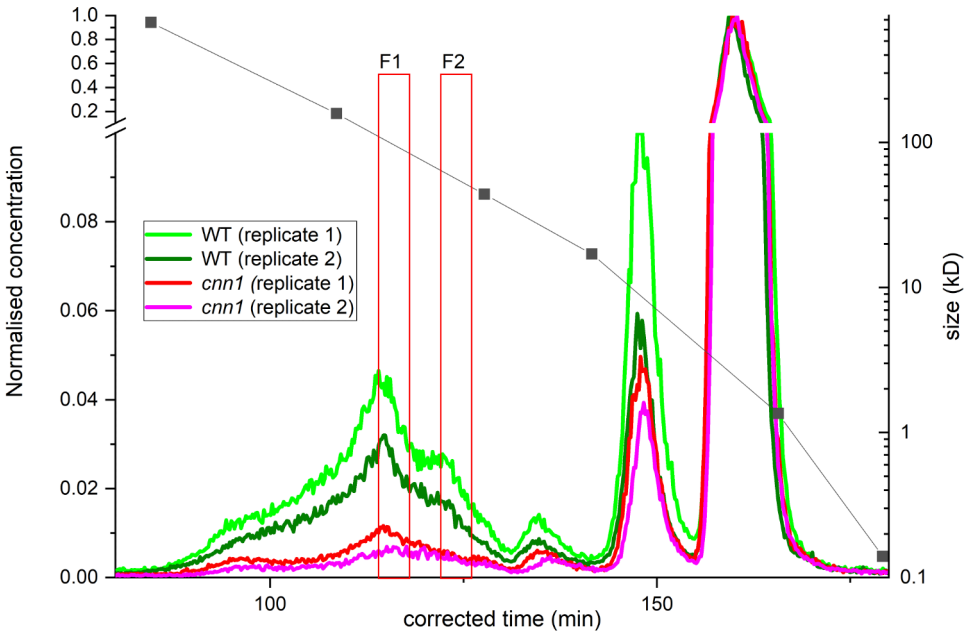
F1
F2
WT (replicate 1)
WT (replicate 2)
cnn1 (replicate 1)
cnn1 (replicate 2)
Normalised concentration
size (kD)
corrected time (min)

B **C**

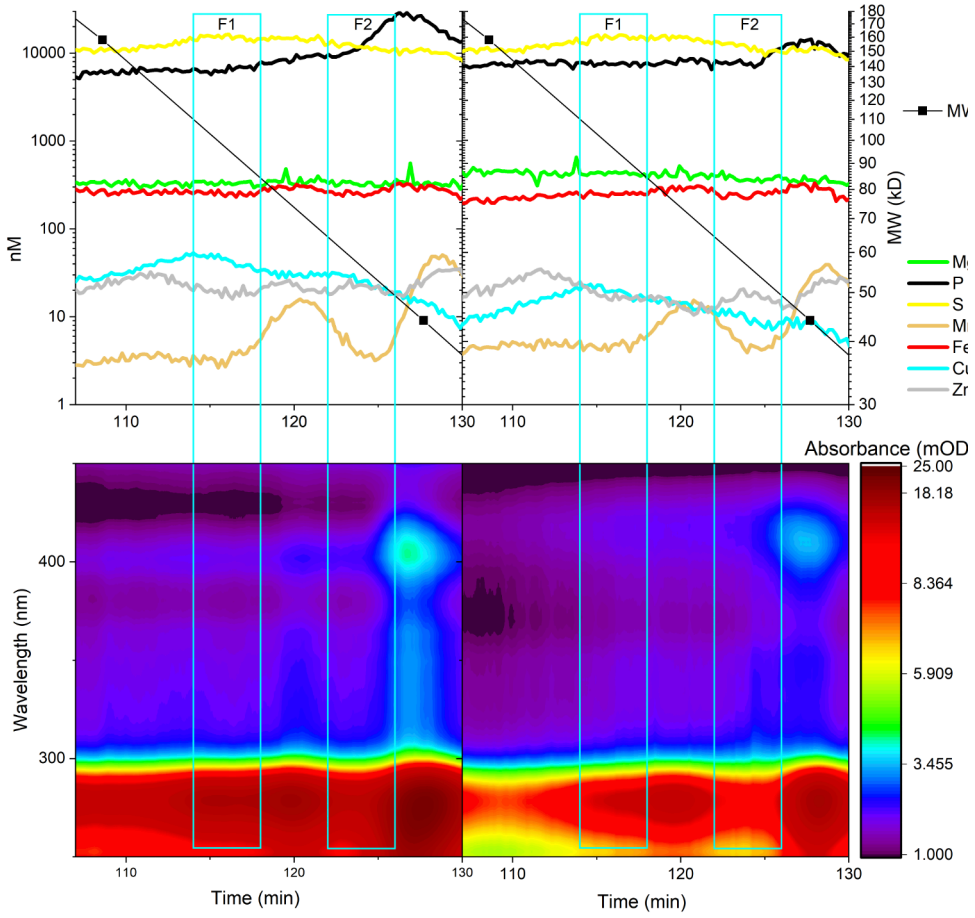
F1
F2
nM
MW (kD)
Absorbance (mOD
Wavelength (nm)
Time (min)
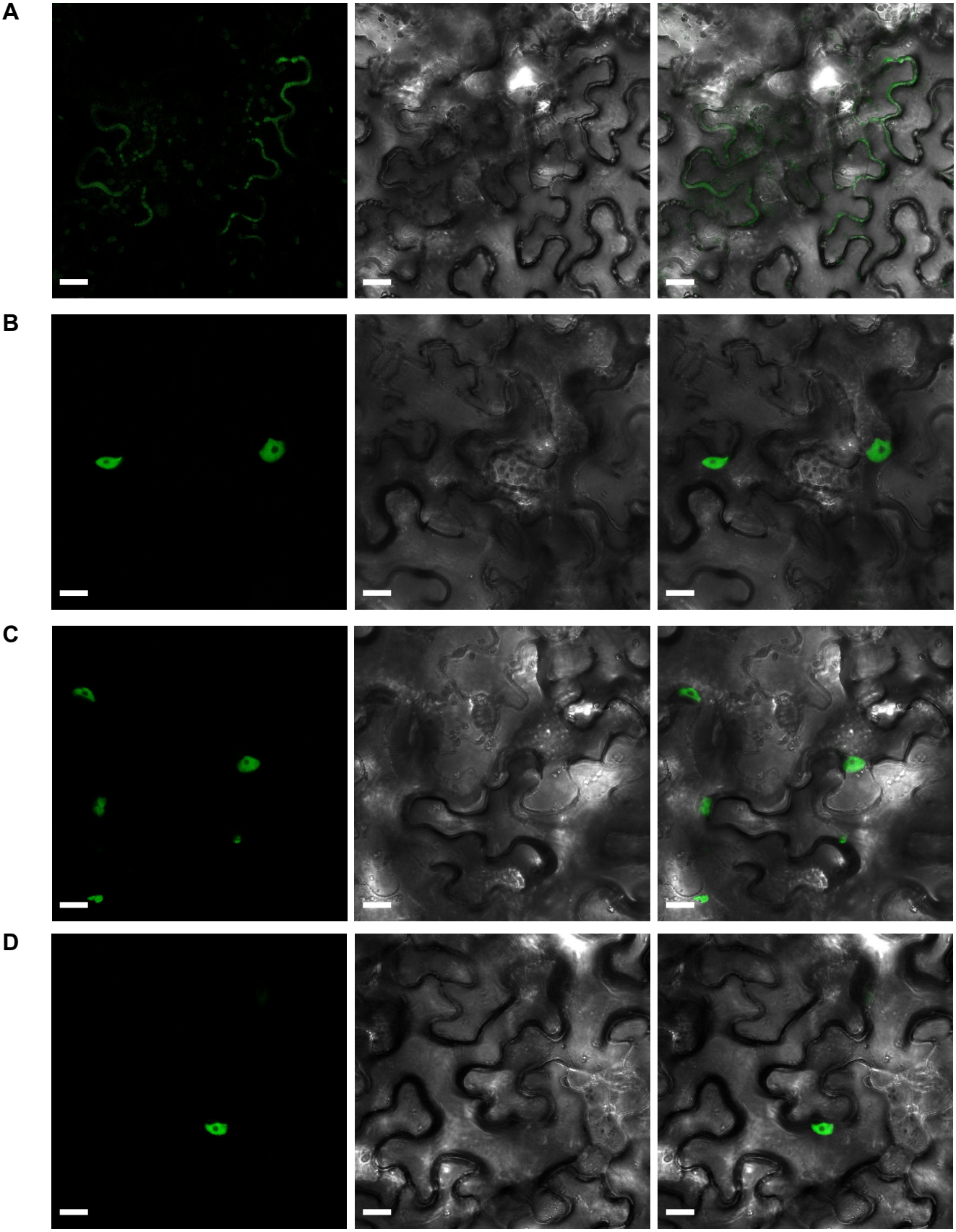
Figure 7